Rapid Communications

Gate tunable optical absorption and band structure of twisted bilayer graphene

Kwangnam Yu,[1] Nguyen Van Luan,[2] Taesoo Kim,[2] Jiwon Jeon,[1] Jiho Kim,[1] Pilkyung Moon,[3,4,5,*] Young Hee Lee,[2,†] and E. J. Choi[1,‡]

[1]*Department of Physics, University of Seoul, Seoul 130-743, Korea*

[2]*Center for Integrated Nanostructure Physics, Institute for Basic Science (IBS), Sungkyunkwan University, Suwon 16419, Korea*

[3]*New York University Shanghai and NYU-ECNU Institute of Physics at NYU Shanghai, Shanghai, China*

[4]*Department of Physics, New York University, New York, USA*

[5]*State Key Laboratory of Precision Spectroscopy, East China Normal University, Shanghai, China*

(Received 1 April 2019; published 21 June 2019)

We report the infrared transmission measurement on electrically gated twisted bilayer graphene. The optical absorption spectrum clearly manifests dramatic changes such as the splitting of the interlinear-band absorption step, the shift of the inter-van Hove singularity transition peak, and the emergence of a very strong intravalence (intraconduction) band transition. These anomalous optical behaviors demonstrate consistently a nonrigid band structure modification created by ion-gel gating through layer-dependent Coulomb screening. We propose that this screening-driven band modification is a universal phenomenon that persists to other bilayer crystals in general, establishing electrical gating as a versatile technique to engineer band structures and to create different types of optical absorptions that can be exploited in electro-optical device applications.

DOI: 10.1103/PhysRevB.99.241405

Introduction. The chemical potential μ of two-dimensional (2D) materials composed of one or a few atomic layers exhibits a marked shift by electrical gating due to their ultrathin sample thickness [1–5], thus manifesting numerous novel optical properties under an external bias. In monolayer graphene, for example, the universal optical conductivity under the linear-band regime $\sigma_{\text{mono}} = e^2/4\hbar$ [6] can be tailored at a certain photon energy E by controlling μ [7–9], allowing for a graphene-based optical modulator [10]. The electrical tuning of optical absorption is not limited to monolayer graphene but was also observed in other two-dimensional materials such as Bernal-stacked bilayer graphene and black phosphorus [11–16].

Twisted bilayer graphene (TBG), two sheets of graphene stacked with a twist angle θ, has attracted a great deal of attention due to the fascinating physics such as the moiré superlattice, Hofstadter butterfly, and the emergence of two-dimensional superconductivity [17–20]. When the Fermi energy lies at the charge neutrality point ($\mu = 0$), the low-energy optical spectrum of TBG is characterized by the linear-band absorption from the two graphene layers [indicated by the red arrows in Fig. 1(b), LB hereafter], yielding $2\sigma_{\text{mono}}$. At higher energies, however, the interlayer interaction hybridizes the LBs of the two graphene layers and yields a band anticrossing as illustrated in Fig. 1(b) [21–25]. Although the transition between the saddle-point van Hove singularities (vHs), i.e., $\text{vHs}_2 \rightarrow \text{vHs}_1$, is exactly forbidden by the lattice symmetry [25], the transition between vHs and the band edge (BE) of the second band exhibits a prominent absorption peak coming from the large joint density of states [blue arrows in Fig. 1(b), peak-α hereafter] [24–27].

It is expected that the optical absorption spectrum of TBG under electrical gating will exhibit rich physics compared to that of monolayer graphene. For example, if μ reaches vHs_2 (vHs_1), either of the interband transitions' peak-α will vanish and a new intravalence (intraconduction) band transition, such as $\text{BE}_2 \rightarrow \text{vHs}_2$ ($\text{vHs}_1 \rightarrow \text{BE}_1$), will emerge due to the depletion of an electron (hole). However, such dramatic changes have yet to be experimentally observed. Here, we report an infrared transmission measurement of gated TBG, and show the optical absorption spectrum with varying μ over a wide range. Our result demonstrates that the electrical gating leads to a significant modification of the band structures, in addition to the μ shift, by creating an interlayer potential asymmetry between the two graphene layers. We further elucidate the full nonrigid band modification schemes and discuss its implication on optical device applications.

Experiment. To make a TBG sample, we first prepared a single-domain monolayer graphene by chemical vapor deposition (CVD) on a single-crystal Cu substrate [28]. Then, a pregrown second graphene sheet was transferred on top of the first one by the bubbling and alignment technique [29]. The TBG sheet was transferred onto a SiO_2/Si substrate for further optical measurement. We chose a lightly p-doped Si substrate (resistivity $\sim$10 Ω cm) which is IR transparent, which allowed us conduct the transmission measurements [30]. To perform the ion-gel gating on the TBG, a mixture of ethyl-methylimidazolium bis(trifluoromethylsulfonyl)imide ([EMIM][TFSI]) ionic liquid, polystyrene-poly(methyl methacrylate)-polystyrene (PS-PMMA-PS) triblock copolymer, and ethyl acetate solvent (weight ratio = 0.1 : 0.9 : 9) was prepared and spin coated on the sample [31]. Optical transmittance was measured using a microscopic Fourier transform infrared (FTIR) device (Bruker, Hyperion 2000) for an infrared frequency range on five samples with different θ's. The optical conductivity

*pilkyung.moon@nyu.edu
†leeyoung@skku.edu
‡echoi@uos.ac.kr

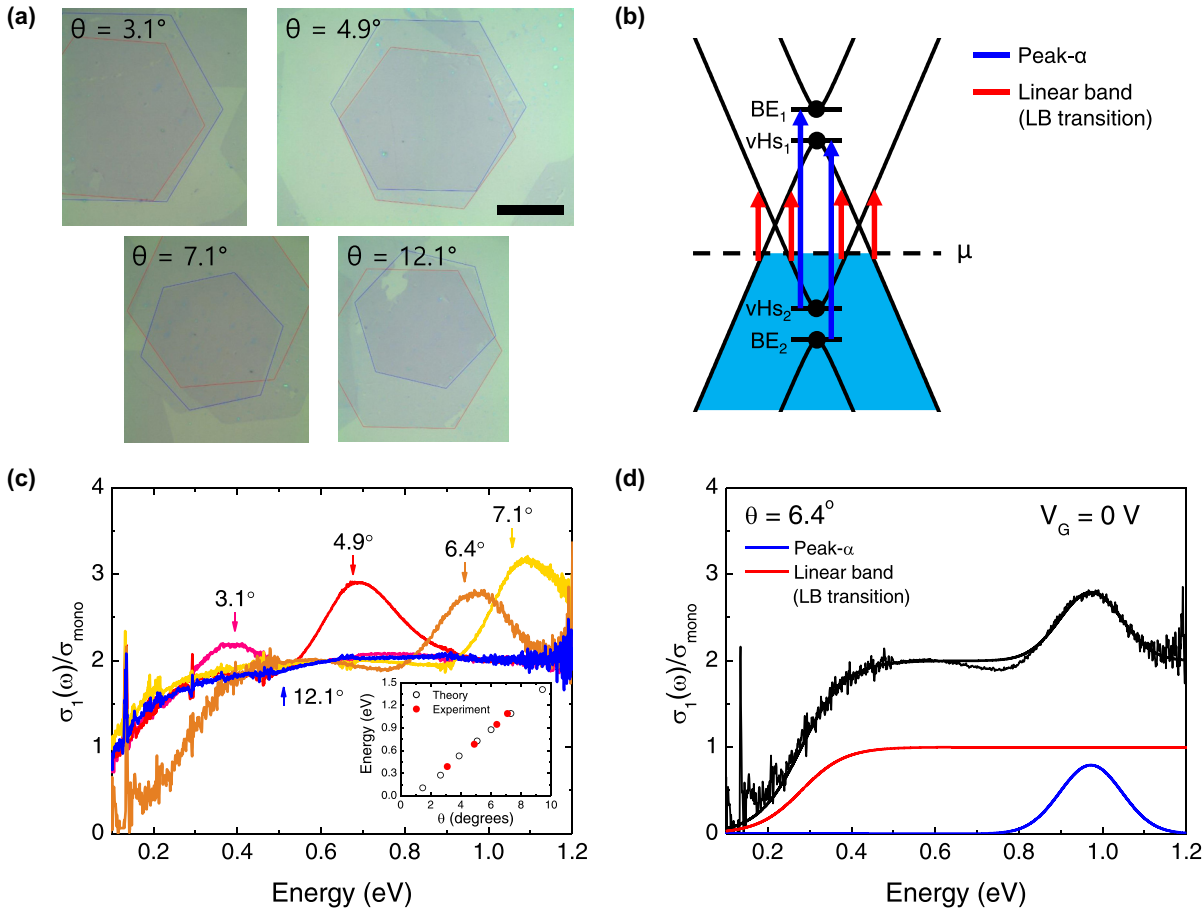

FIG. 1. Optical absorption of ungated TBG. (a) Optical images of TBG samples with different twisted angles θ. The scale bar is 20 μm. (b) Electronic band diagram of TBG. BE and vHs stand for the band edge of the second band and the saddle-point van Hove singularity, respectively. Two kinds of optical transitions are activated as shown by the red and blue arrows. (c) Optical conductivity $\sigma_1(\omega)$ of the five TBG samples. The peak-α shifts to higher energy as θ increases. The sharp peak at $E = 0.13$ eV is an artifact due to optical phonon absorption of SiO_2. The inset compares the measured peak position with the theoretical prediction [25]. (d) The $\sigma_1(\omega)$ can be fit in terms of the LB transition (red curve) and peak-α (blue curve).

$\sigma_1(\omega)$ of TBG was extracted by fitting the raw data using the multilayer Kramers-Kronig analysis program RefFIT [32].

Results. In Fig. 1(c), we show the optical conductivity $\sigma_1(\omega)$ of TBG with various rotation angles (see Supplemental Fig. S1 for the raw data [33]). The $\sigma_1(\omega)$ spectrum shows two distinct interband transitions described in Fig. 1(b): (i) the frequency-independent conductivity $2\sigma_{\text{mono}}$ which comes from the LB transition (red arrows), and (ii) the prominent absorption peak-α which comes from the transitions $\text{vHs}_2 \rightarrow \text{BE}_1$ and $\text{BE}_2 \rightarrow \text{vHs}_1$ [24,25]. Peak-α blueshifts as θ increases [Fig. 1(c) and inset], since the two Dirac cones in Fig. 1(b) move apart, increasing the energy of the vHs [25]. Figure 1(d) shows the fitting of the conductivity with LB and peak-α using a model function

$$\sigma_1(\omega, \mu) = 2\sigma_{\text{LB}}(\omega, \mu) + \sigma_\alpha(\omega). \tag{1}$$

Here, the factor 2 comes from the layer degeneracy, and the LB-transition conductivity for each layer is given by

$$\sigma_{\text{LB}}(\omega, \mu) = \sigma_{\text{mono}}\left[\tanh\left(\frac{\hbar\omega + 2\mu}{4k_B T}\right) + \tanh\left(\frac{\hbar\omega - 2\mu}{4k_B T}\right)\right]\Big/2, \tag{2}$$

where μ (=0.28 eV) and T (=300 K) are the chemical potential and temperature, respectively [8]. For peak-α, we use the standard Gaussian function

$$\sigma_\alpha(\omega) = \frac{S_\alpha}{\sqrt{2\pi\Gamma_\alpha^2}} \exp\left[-\frac{(\hbar\omega - E_\alpha)^2}{2\Gamma_\alpha^2}\right], \tag{3}$$

where S_α, E_α, and Γ_α stand for the intensity, energy, and broadening of the peak, respectively. The model function fits very well the measured conductivity except for a minor discrepancy at 0.76 eV, where the latter discrepancy is due to the deactivation of the LB transition in the small region of K space where the hybridization gap is opened, as theoretically predicted [25].

We prepared an ion-gel gating circuit on the $\theta = 6.4°$ sample as schematically shown in Fig. 2(a), and measured the optical transmittance by varying the bias voltage V_G over $-2\text{ V} < V_G < 2\text{ V}$. The reference charge neutral point V_{CNP} of this TBG sample is 0.84 V, as we will show later in Fig. 4(a). Figure 2(b) shows the V_G-driven change of $\sigma_1(\omega)$ for the hole-doping regime, $-2\text{ V} < V_G < V_{\text{CNP}}$. In a rigid band picture, the absorption edge of the LB transition σ_{LB} will remain sharp, and both the energy and intensity of peak-α

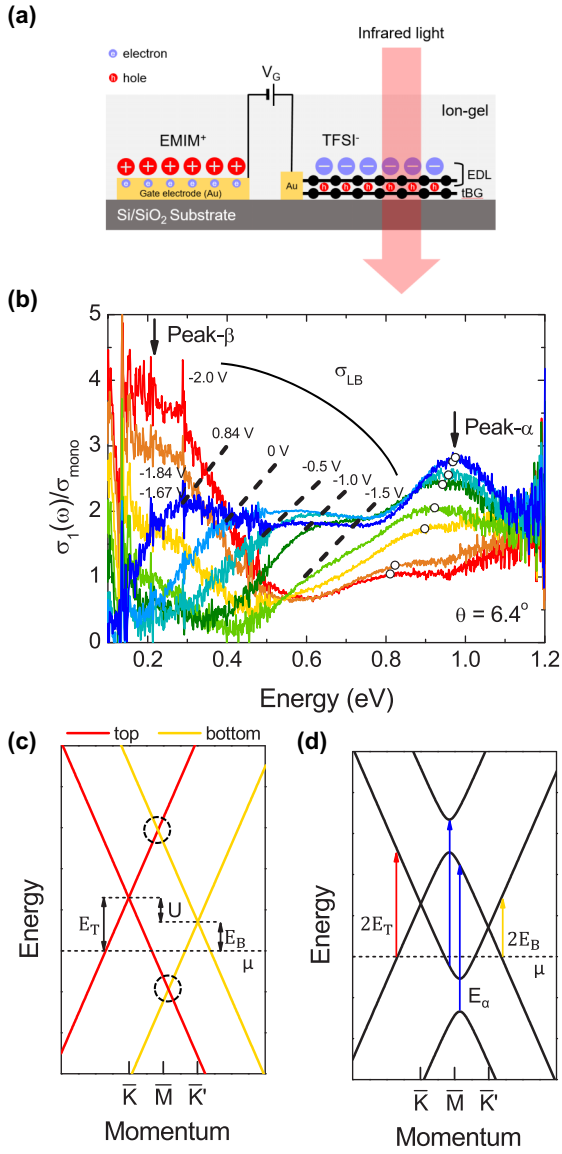

FIG. 2. Optical absorption of ion-gel gated TBG. (a) Schematic view of the ion-gel gating circuit and the infrared transmission measurement. (b) Optical conductivity of gated TBG ($\theta = 6.4°$) for various gate voltages V_G. The gate-driven changes of the LB transition, peak-α, and peak-β are observed and discussed in detail in the text. (c) The band structure of TBG under gating. The top band and bottom band shift by E_T and E_B, respectively. U is their difference, $U = E_T - E_B$. Here, the gap opening is omitted for clarity. (d) Optical transitions change in the gated TBG compared with the ungated one as a result of the band shifts.

will remain unchanged with V_G until μ reaches vHs_2. The absorption profile in Fig. 2(b), however, shows that (i) the absorption edge of σ_{LB} shows a considerable broadening and shifts to higher energy, and (ii) peak-α shifts to lower energy while its intensity is reduced markedly. Thus, our observations provide clear evidence that the band structure of TBG varies with gating. Such a drastic change of the band structure, i.e., a nonrigid band modification, mainly arises from the charge screening by the graphene layer. The two graphene layers have an asymmetric charge density distribution, since the electric field from the ion gel is screened by the charge at the top graphene layer. Thus, the bands of the top and bottom layers shift by a different amount, E_T and E_B, respectively, leading to an asymmetric potential profile as sketched in Fig. 2(c). Figure 2(d) shows the effect of the asymmetric band shift on the optical transitions. First, the absorption edge of the LB transition splits into $2E_T$ and $2E_B$ for the two graphene layers rather than being degenerated, demonstrating that the band shift difference U can be determined once the LB-transition energies are measured from $U = E_T - E_B$. Second, the hybridization gap in the conduction band and valence band shift from their ungated position $\bar{M}$ to opposite directions, $\bar{K}$ and $\bar{K}'$, respectively. As result, peak-α energy is reduced. Also, since the optical transition can no longer simultaneously involve vHs and BE, the intensity of peak-α is decreased. When μ passes vHs_2 by strong gating, a new absorption peak (peak-β hereafter) emerges due to the intravalence band transition as shown in Fig. 3(f). To reflect these nonrigid band features, we fit the absorption spectrum to

$$\sigma_1(\omega) = \sum_{i=T,B} \sigma_{LB}(\omega, E_i) + \sum_{j=\alpha,\beta} \sigma_j(\omega) + \sigma_D(\omega). \quad (4)$$

The first term in Eq. (4) is summed over the top (T) and bottom (B) layers, and represents the LB transition from two shifted Dirac cones. The second term refers to the vHs-BE transitions peak-α and peak-β, in the form of the Gaussian function with intensity S_β, energy E_β, and broadening Γ_β of the peak, and the last term $\sigma_D(\omega)$ represents the Drude (intraband) conductivity of Dirac carrier [30,34,35].

Figure 3 shows the fitting result for three representative V_G's corresponding to CNP (=0.84 V), intermediate (−1.3 V), and strong (−2 V) gating. The fits are in fair agreement with the measured optical absorption spectrum as shown in Figs. 3(a), 3(c) and 3(e), and reveals the relevant parameters $E_{T/B}$, $S_{\alpha/\beta}$, $E_{\alpha/\beta}$, and $\Gamma_{\alpha/\beta}$. Figures 3(b), 3(d) and 3(f) show the band structure for each V_G that reproduces the optical transition energies as fitted.

Figure 4 displays the fitting parameters as a function of V_G. Figure 4(a) shows that the band shifts E_T and E_B increase along with gating, consistent with the band evolution in Figs. 3(b)–3(f). Here, we determine the interlayer potential difference U from E_T and E_B by calculating $U = E_T - E_B$. We also show E^* which refers to the lower bound of the LB transition of the top band at $\bar{M}$ as depicted in Fig. 3(d). E^* is smaller than E_T due to the gap opening. By refining σ_{LB} in the fit, we found the lower bound of the LB transition, $2E^*$, for a gating range of $V_G < -1$ V (see Supplemental Fig. S2 for details [33]). At weak gating, E^* is close to the value of E_T but it becomes closer to the value of E_B as μ reaches vHs_2. Thus, E^* and E_B indicate that μ reaches vHs_2 at $V_G = -1.5$ V. Figure 4(b) shows the V_G dependence of the energy and intensity of peak-α. The peak energy E_α decreases with V_G. Figures 2(c) and 2(d) show that the amount of the gate-driven change of E_α, ΔE_α [$\equiv E_\alpha(0) - E_\alpha(V_G)$], is approximately equal to U. Our calculation of U (see Supplemental Fig. S3 for details [33]) is compared with the U obtained from σ_{LB} in Fig. 4(a). The two U's calculated from independent optical transitions

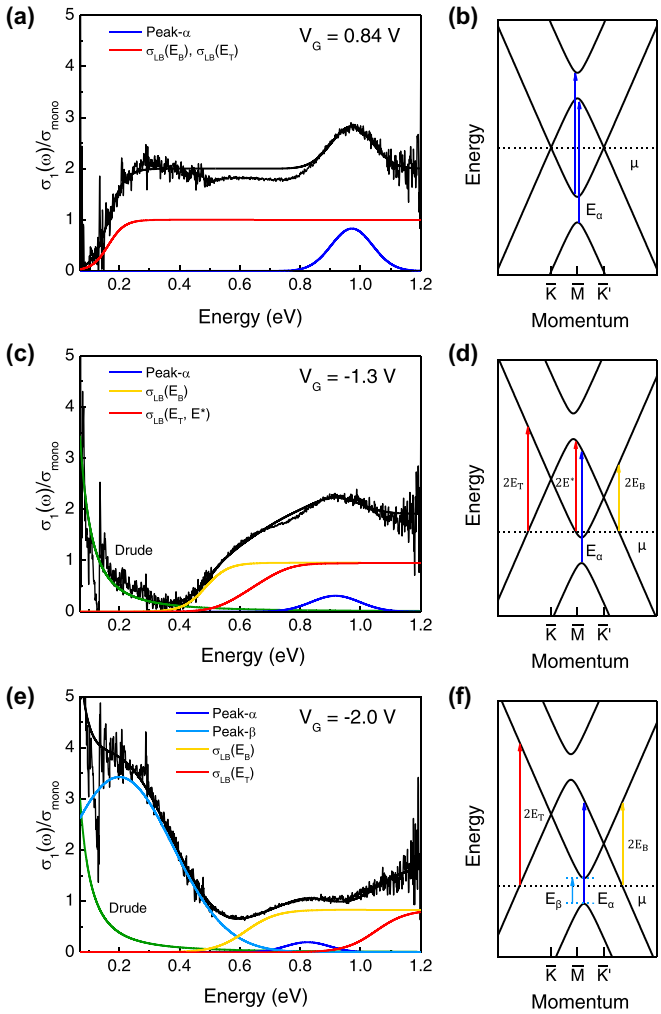

FIG. 3. Gate-driven evolution of the optical conductivity (left column) and the band structure (right column). (a), (c), (e) Fit of optical conductivity for $V_G = 0.84$, -1.3, and -2.0 V. (b), (d), (f) Nonrigid band evolution and optical transitions for (a), (c), and (e). As V_G is increased, U becomes stronger, and as a result, peak-α transition energy decreases. In (f), the new β transition (sky blue) is activated.

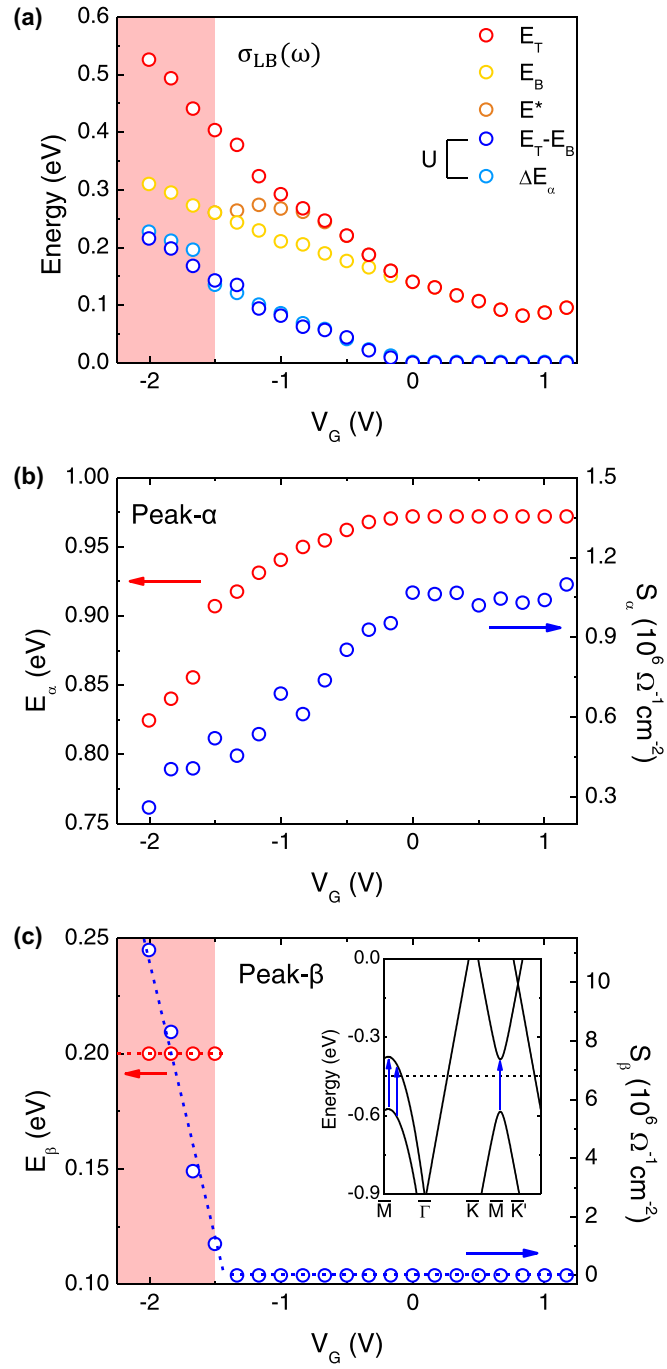

FIG. 4. Fitting result of the peak energy and intensity (a) LB-transition energy E_T (and E^*) for the top graphene, and E_B for bottom graphene. U is calculated from the LB transition and, independently, from the peak-α shift $U = E_\alpha(0) - E_\alpha(V_G)$. (b) Peak energy E_α and strength S_α of peak-α. (c) E_β and S_β of peak-β. The inset shows the band structure along $\bar{M} \to \bar{\Gamma}$ and $\bar{M} \to \bar{K}$, where the arrows emphasize the optical criticality of peak-β.

σ_{LB} and peak-α are consistent with each other for the whole range of V_G, demonstrating that the nonrigid band picture can describe the physical properties of the gated TBG very well. The intensity of peak-α (S_α) is proportional to the optical transition matrix element (M_{if}) and the density of the initial ρ_i and final states ρ_f. At $V_G = V_{CNP}$, S_α is very large since the vHs and BE align in the Brillouin zone, giving a very large $\rho_i\rho_f$. However, S_α decreases as we apply the gate bias since (i) the vHs and BE no longer align due to $U \neq 0$, and (ii) one of the two α-transition channels becomes silent when μ enters the gap [Figs. 3(b), 3(d) 3(f), and 4(b)]. Figure 4(c) shows the V_G dependence of the intravalence band transition, peak-β. Peak-β is silent until μ reaches vHs_2, i.e., V_G reaches -1.5 V. Once the transition is activated, however, it gives a strong absorption peak at the energy corresponding to the magnitude of the band opening, i.e., the energy difference between vHs_2 and BE_2. Theoretical investigation predicts that the amount of band opening equals $2u_0$, where

$$u_0 = \frac{1}{\sqrt{S\tilde{S}}} \int T(\mathbf{r} + d_z\mathbf{e}_z)e^{-i\mathbf{K}\cdot\mathbf{r}}d\mathbf{r} \tag{5}$$

is the measure of the interlayer interaction strength [21,24,25]. Here, S and $\tilde{S}$ are the area of each graphene layer, $T(\mathbf{R})$ is the

transfer integral between the atoms at a relative vector of $\mathbf{R}$, d_z is the distance between the two layers, $\mathbf{K}$ is the Dirac point of graphene, and the integral in $\mathbf{r}$ is taken over the total two-dimensional space. The band structures of low-angle TBGs ($\theta \leqslant 10^\circ$) are very well described by this single parameter, u_0. The energy of peak-β, $E_\beta = 0.2$ eV ($=2u_0$) measured in this work, provides important information about its value of 0.1 eV, which is consistent with the theoretical expectation of $u_0 \sim 0.110$ eV. In addition, Fig. 4(c) shows that the intensity S_β grows rapidly with further gating. This is because the two bands associated with this transition are almost parallel along $\bar{M}$-$\bar{\Gamma}$ see the inset of Fig. 4(c) [36], $\nabla_{\mathbf{K}} E_f \cong \nabla_{\mathbf{K}} E_i$, which give a prominent peak intensity $S_\beta \sim \int_{\mathrm{FS}} \frac{dS}{|\nabla_{\mathbf{K}} E_f - \nabla_{\mathbf{K}} E_i|}$ (FS=Fermi surface). From the band structures, we expect that peak-β will grow further for deeper gating $V_\mathrm{G} < -2$ V. Theoretically t is predicted to be independent on carrier density [36], which is supported by our E_β being constant with V_G.

Discussion. We investigated the optical absorption spectrum of electrically gated TBG. We showed that two different kinds of interband optical transitions take place in TBG, namely, the transition between the linear bands (σ_LB) and that between vHs and the band edge (peak-α). Their behaviors with varying applied bias show clear evidence of the nonrigid band evolution. Specifically, the absorption edge of σ_LB is split into two edges with different energies, indicating that the Dirac cones of the top and bottom layers are shifted by different amounts of energy. In addition, both the energy and intensity of peak-α show marked changes with the gate bias, since the interlayer potential asymmetry breaks the alignment of the vHs and the band edge associated with the hybridization gap changes the band structures from direct to indirectlike. The amounts of interlayer potential asymmetry U extracted from the two independent phenomena, σ_LB and peak-α, were consistent with each other. Besides, we found that a unique intravalence (intraconduction) band transition (peak-β) is activated with further gating. The intensity of peak-β can grow much larger than that of peak-α, and the energy of peak-β is, unlike peak-α, less sensitive to the gate bias after it is activated. Moreover, the energy of peak-β provides important information on the interlayer interaction strength, which is essential in revealing the full band structures of tBG.

Gate tunable optical absorption has a significant impact on electro-optical applications. For peak-β, TBG can either transmit ($S_\beta = 0$) or strongly absorb (large S_β) the infrared light at $E_\beta = 0.2$ eV by V_G control, which can be used for tunable modulators or filters. As for peak-α, this peak absorbs visible light (red, green, blue) for TBG samples in the range of $\theta = 13^\circ$–17° [25]. There, the electrical gating is of particular interest because the gate-driven peak shift/suppression may lead to a possible color change. Further electro-optic applications could be found by extending the notion of tunable band structures to other bilayer materials. Recent studies showed that a 2D material can have many kinds of band structures, linear or parabolic, metallic or insulating, direct or indirect gaps, and so on [37–41]. When two such monolayers M1 and M2 form a bilayer composite, M1/M2, we can assume that the same layer-dependent screening principle applies, i.e., the M1 band shifts relative to the M2 band when gated, which can create different kinds of optical changes other than what we observed in TBG, which will be interesting to investigate theoretically and experimentally.

Acknowledgments. This work was supported by the National Research Foundation of Korea (NRF) grant funded by the Korea government (MSIT) (No. 2017R1A2B4007782). P.M. was supported by NYU Shanghai (Start-Up Funds), NYU-ECNU Institute of Physics at NYU Shanghai, New York University Global Seed Grants for Collaborative Research. The work at SKKU was supported by the Institute for Basic Science (IBS-R011-D1).

[1] K. S. Novoselov, A. K. Geim, S. V. Morozov, D. Jiang, Y. Zhang, S. V. Dubonos, I. V. Grigorieva, and A. A. Firsov, Science **306**, 666 (2004).
[2] K. S. Novoselov, A. K. Geim, S. V. Morozov, D. Jiang, M. I. Katsnelson, I. V. Grigorieva, S. V. Dubonos, and A. A. Firsov, Nature (London) **438**, 197 (2005).
[3] J. B. Oostinga, H. B. Heersche, X. Liu, A. F. Morpurgo, and L. M. K. Vandersypen, Nat. Mater. **7**, 151 (2008).
[4] M. M. Furchi, D. K. Polyushkin, A. Pospischil, and T. Mueller, Nano Lett. **14**, 6165 (2014).
[5] D. Costanzo, S. Jo, H. Berger, and A. F. Morpurgo, Nat. Nanotechnol. **11**, 339 (2016).
[6] R. R. Nair, P. Blake, A. N. Grigorenko, K. S. Novoselov, T. J. Booth, T. Stauber, N. M. R. Peres, and A. K. Geim, Science **320**, 1308 (2008).
[7] Z. Q. Li, E. A. Henriksen, Z. Jiang, Z. Hao, M. C. Martin, P. Kim, H. L. Stormer, and D. N. Basov, Nat. Phys. **4**, 532 (2008).
[8] K. F. Mak, M. Y. Sfeir, Y. Wu, C. H. Lui, J. A. Misewich, and T. F. Heinz, Phys. Rev. Lett. **101**, 196405 (2008).
[9] T. Jiang, D. Huang, J. Cheng, X. Fan, Z. Zhang, Y. Shan, Y. Yi, Y. Dai, L. Shi, K. Liu, C. Zeng, J. Zi, J. E. Sipe, Y.-R. Shen, W.-T. Liu, and S. Wu, Nat. Photonics **12**, 430 (2018).
[10] M. Liu, X. Yin, E. Ulin-Avila, B. Geng, T. Zentgraf, L. Ju, F. Wang, and X. Zhang, Nature (London) **474**, 64 (2011).
[11] Y. Zhang, T.-T. Tang, C. Girit, Z. Hao, M. C. Martin, A. Zettl, M. F. Crommie, Y. R. Shen, and F. Wang, Nature (London) **459**, 820 (2009).
[12] Z. Q. Li, E. A. Henriksen, Z. Jiang, Z. Hao, M. C. Martin, P. Kim, H. L. Stormer, and D. N. Basov, Phys. Rev. Lett. **102**, 037403 (2009).
[13] A. Chernikov, A. M. van der Zande, H. M. Hill, A. F. Rigosi, A. Velauthapillai, J. Hone, and T. F. Heinz, Phys. Rev. Lett. **115**, 126802 (2015).
[14] W. S. Whitney, M. C. Sherrott, D. Jariwala, W.-H. Lin, H. A. Bechtel, G. R. Rossman, and H. A. Atwater, Nano Lett. **17**, 78 (2016).
[15] L. Ju, L. Wang, T. Cao, T. Taniguchi, K. Watanabe, S. G. Louie, F. Rana, J. Park, J. Hone, F. Wang, and P. L. McEuen, Science **358**, 907 (2017).

[16] K. Yao, A. Yan, S. Kahn, A. Suslu, Y. Liang, E. S. Barnard, S. Tongay, A. Zettl, N. J. Borys, and P. J. Schuck, Phys. Rev. Lett. **119**, 087401 (2017).
[17] T. Ohta, J. T. Robinson, P. J. Feibelman, A. Bostwick, E. Rotenberg, and T. E. Beechem, Phys. Rev. Lett. **109**, 186807 (2012).
[18] R. Bistritzer and A. H. MacDonald, Phys. Rev. B **84**, 035440 (2011).
[19] P. Moon and M. Koshino, Phys. Rev. B **85**, 195458 (2012).
[20] Y. Cao, V. Fatemi, S. Fang, K. Watanabe, T. Taniguchi, E. Kaxiras, and P. Jarillo-Herrero, Nature (London) **556**, 43 (2018).
[21] J. M. B. Lopes dos Santos, N. M. R. Peres, and A. H. Castro Neto, Phys. Rev. Lett. **99**, 256802 (2007).
[22] E. J. Mele, Phys. Rev. B **81**, 161405(R) (2010).
[23] J. M. B. Lopes dos Santos, N. M. R. Peres, and A. H. Castro Neto, Phys. Rev. B **86**, 155449 (2012).
[24] C. J. Tabert and E. J. Nicol, Phys. Rev. B **87**, 121402(R) (2013).
[25] P. Moon and M. Koshino, Phys. Rev. B **87**, 205404 (2013).
[26] R. W. Havener, Y. Liang, L. Brown, L. Yang, and J. Park, Nano Lett. **14**, 3353 (2014).
[27] C.-J. Kim, A. Sánchez-Castillo, Z. Ziegler, Y. Ogawa, C. Noguez, and J. Park, Nat. Nanotechnol. **11**, 520 (2016).
[28] V. L. Nguyen, B. G. Shin, D. L. Duong, S. T. Kim, D. Perello, Y. J. Lim, Q. H. Yuan, F. Ding, H. Y. Jeong, H. S. Shin, S. M. Lee, S. H. Chae, Q. A. Vu, S. H. Lee, and Y. H. Lee, Adv. Mater. **27**, 1376 (2015).
[29] V. L. Nguyen, D. J. Perello, S. Lee, C. T. Nai, B. G. Shin, J.-G. Kim, H. Y. Park, H. Y. Jeong, J. Zhao, Q. A. Vu, S. H. Lee, K. P. Loh, S.-Y. Jeong, and Y. H. Lee, Adv. Mater. **28**, 8177 (2016).
[30] J. Horng, C.-F. Chen, B. Geng, C. Girit, Y. Zhang, Z. Hao, H. A. Bechtel, M. Martin, A. Zettl, M. F. Crommie, Y. R. Shen, and F. Wang, Phys. Rev. B **83**, 165113 (2011).
[31] B. J. Kim, H. Jang, S.-K. Lee, B. H. Hong, J.-H. Ahn, and J. H. Cho, Nano Lett. **10**, 3464 (2010).
[32] A. B. Kuzmenko, Rev. Sci. Instrum. **76**, 083108 (2005).
[33] See Supplemental Material at http://link.aps.org/supplemental/10.1103/PhysRevB.99.241405 for additional data of the ion-gel gated TBG.
[34] C. Lee, J. Y. Kim, S. Bae, K. S. Kim, B. H. Hong, and E. J. Choi, Appl. Phys. Lett. **98**, 071905 (2011).
[35] K. Yu, J. Kim, J. Y. Kim, W. Lee, J. Y. Hwang, E. H. Hwang, and E. J. Choi, Phys. Rev. B **94**, 235404 (2016).
[36] P. Moon, Y.-W. Son, and M. Koshino, Phys. Rev. B **90**, 155427 (2014).
[37] A. Kuc, N. Zibouche, and T. Heine, Phys. Rev. B **83**, 245213 (2011).
[38] T. Cheiwchanchamnangij and W. R. L. Lambrecht, Phys. Rev. B **85**, 205302 (2012).
[39] F. Zahid, L. Liu, Y. Zhu, J. Wang, and H. Guo, AIP Adv. **3**, 052111 (2013).
[40] C. Ruppert, O. B. Aslan, and T. F. Heinz, Nano Lett. **14**, 6231 (2014).
[41] A. N. Rudenko and M. I. Katsnelson, Phys. Rev. B **89**, 201408(R) (2014).